chemistry

MDPI

Article

Synthesis of Metal Nanoparticles via *Pulicaria undulata* and an Evaluation of Their Antimicrobial, Antioxidant, and Cytotoxic Activities

Yasser A. El-Amier [1,*], Balsam T. Abduljabbar [1], Mustafa M. El-Zayat [2,3], Tushar C. Sarker [4] and Ahmed M. Abd-ElGawad [5,*]

1 Botany Department, Faculty of Science, Mansoura University, Mansoura 35516, Egypt; dr.balsamtareq@gmail.com
2 Department of Biology, Faculty of Science, New Mansoura University, New Mansoura City 35511, Egypt; mustafa.mohsen@nmu.edu.eg
3 Unit of Genetic Engineering and Biotechnology, Mansoura University, Mansoura 35516, Egypt
4 Texas A&M AgriLife Research Center, Overton, TX 75684, USA; tushar.sarker@ag.tamu.edu
5 Plant Production Department, College of Food & Agriculture Sciences, King Saud University, P.O. Box 2460, Riyadh 11451, Saudi Arabia
* Correspondence: yasran@mans.edu.eg (Y.A.E.-A.); aibrahim2@ksu.edu.sa (A.M.A.-E.); Tel.: +20-101-722-9120 (Y.A.E.-A.); +966-562680864 (A.M.A.-E.)

Abstract: Nanoparticle engineering via plants (green synthesis) is a promising eco-friendly technique. In this work, a green protocol was applied to the preparation of silver, zinc, and selenium nanoparticle solutions supported by the extracted aerial parts of *Pulicaria undulata*. The formation of nanoparticles in the solution was characterized using phytochemical analysis, and UV-visible, TEM, and zeta-potential spectroscopy. In addition, various biological activities were investigated for the extract of *P. undulata* and the produced nanoparticles (selenium, silver, and zinc), including antioxidant, antimicrobial, and cytotoxic activities. The volatile components of the extracted constitute verified the fact that twenty-five volatile components were characterized for the majority of abundant categories for the fatty acids, esters of fatty acids (59.47%), and hydrocarbons (38.19%) of the total area. The antioxidant activity of *P. undulata* extract and metal nanoparticles was assessed using DPPH assay. The results indicated reduced potency for the metal nanoparticles' solutions relative to the results for the plant extract. The cytotoxicity of the investigated samples was assessed using an MTT assay against various tumor and normal cell lines with improved cytotoxic potency of the solutions of metal nanoparticles, compared to the plant extract. The antimicrobial activity was also estimated against various bacterial and fungal species. The results confirmed amended potency for inhibiting the growth of microbial species for the solutions of metal nanoparticles when compared to the extracted aerial parts of the plant. The present study showed that green synthetized nanoparticles using *P. undulata* have various potential bioactivities.

Keywords: desert golden daisy; nanomedicine; GC-MS analysis; bioactivity; green synthesis

check for updates

Citation: El-Amier, Y.A.; Abduljabbar, B.T.; El-Zayat, M.M.; Sarker, T.C.; Abd-ElGawad, A.M. Synthesis of Metal Nanoparticles via *Pulicaria undulata* and an Evaluation of Their Antimicrobial, Antioxidant, and Cytotoxic Activities. *Chemistry* **2023**, *5*, 2075–2093. https://doi.org/10.3390/chemistry5040141

Academic Editor: Sofia Lima

Received: 8 August 2023
Revised: 16 September 2023
Accepted: 25 September 2023
Published: 26 September 2023

1. Introduction

In communities with limited resources, traditional medicine has continued to be the most accessible and reasonably priced form of therapy [1]. Additionally, the focus on the usage of medicinal herbs had hitherto been on illness treatment rather than prevention. Any plant that has compounds that can be utilized therapeutically, or which is the precursors for the synthesis of useful drugs, is a medicinal plant [2,3].

The genus *Pulicaria*, family Asteraceae, is signified by ca. 100 species. *Pulicaria undulata* (L.) C.A.Mey. (syn. *Pulicaria crispa* (Forssk.) Oliv.) is one of the wildest plants grown in the Egyptian desert and is usually applied as a traditional herbal therapy [4,5]. Recently, Mustafa et al. [6] have reported the utility of GC-MS analysis for the characterization of the chemical components of the essential oil of the extracted *P. undulata*. Also, a comparative study of two ecospecies of essential oils of *P. undulata* showed the effect of varied environmental and climatic conditions on the essential oil composition [7]. Following this route, sixty-four volatile components were characterized with the majority having an abundance of monoterpenes and aromatic compounds, with these forming 82.8% of the total area percentage. The extracted oil of *P. undulata* has been found to have an antioxidant character, cytotoxic activity against A375, T98G, and HCT116 tumor cell lines, and anti-acetylcholinesterase activity [6]. The plant extract also demonstrated antimicrobial activities against a variety of microbial species [8,9], as well as showing allelopathic activity [7] and anticancer activity [10,11]. Also, the antiproliferative, antioxidant, and enzyme inhibition capacities of *P. undulata* were inspected [4], as well as the antifungal activity of the methanol extract [4]. Mohammed, et al. [12] have recently applied the identification of the chemical profile of the water–ethanol extract of *P. undulata* grown in the Saudi Arabian desert to the investigation of the *P. undulata*, which was investigated as an antioxidant and antimicrobial agent, as reported by Foudah, et al. [13]; the volatile chemical components of the petroleum ether extract of the same plant (whole plant) were characterized by GC-MS spectrometry [14]. Ohmic hydrodistillation was applied to the extraction of the essential oil of *P. undulata*, with the aid of an energy-saving green process [15].

Recently, nanotechnology/nanomaterials have attracted the attention of researchers and scientists worldwide, due to their various applications in agriculture, medicine, industry, and pharmaceuticals [16]. These nanomaterials include a broad spectrum of examples with a dimension of 1 to 100 nm, and they are characterized by high surface area [17]. The nanoparticle can be formulated by two approaches; the top-down method and the bottom-up approach. In the top–down method, the nanomaterial is synthesized from large-sized materials that are divided into pieces that develop into nanoparticles, while in the bottom–up method small atoms and molecules are collected to build up nanoparticles [18]. The green/biosynthesis method is among the bottom–up approaches. The green synthesis of nanoparticles has come to be considered a new and promising field for the production of nanomaterials. The green and biocompatible protocols for the preparation of metal/metal oxide nanoparticles from natural plant extracts uses low-cost, readily available materials, less energy, nontoxic materials, efficient eco-friendly products, and prevents or minimizes the use of hazardous products [19,20]. Recently, nanotechnology has developed as one of the most imperative and stimulating leading fields in physics, chemistry, engineering, and biology. In addition, green synthesis has been applied to the preparation of metal nanoparticles using plant extract on a large scale [21]. In this context, few studies dealt with the formulation of nanoparticles using *P. undulata* extract. Dehvari and Ghahghaei [22] studied the ability of an Iranian ecospecies of *P. undulata* for the green synthesis of silver nanoparticles, and evaluated its effect on the amyloid formation in α-lactalbumin and the chaperon action of α-casein. The *P. undulata* collected from Saudi Arabia was used for the synthesis of Au, Ag, and Au-Ag nanoparticles [23], which showed substantial catalytic activity for the reduction of 4-nitrophenol. However, in our survey of the literature, no study dealt with the formulation of nanoparticles using Egyptian ecospecies, and no study formulated the nanoparticles of zinc and selenium at all. Also, the evaluation of the green synthesized nanoparticle via *P. undulata* as an antimicrobial, antioxidant, and cytotoxic agent has not been studied yet. Therefore, the present work aimed to explore and improve the biological profile of the extracted Egyptian *P. undulata* through the utility of nanotechnology in the preparation of metal nanoparticles following a green protocol. The volatile components of the plant extract were characterized using GC-MS spectral analysis. Also, the plant extract and its metal nanoparticles were well characterized using phytochemical and spectral analysis. In addition, the antioxidant, antimicrobial, and cytotoxic activities of this plant and its metal nanoparticles were investigated.

2. Materials and Methods

2.1. Plant Material and Extraction Process

The aerial parts of *P. undulata* were collected from Wadi Araba, located in the northern part of the Eastern Desert of Egypt. The aerial parts include stems, leaves, and inflorescences. The plant materials were consequently cleaned, air-dried, and crushed into small pieces using a grinder. About 10 gm of the plant was retained in a conical flask (250 mL), then methanol (150 mL) was added. The mixture was shaken in a horizontal water bath shaker for four hours at 25 °C and filtered using Whatman filter paper no. 1 (125 mm, Cat No 1001 125, Darmstadt, Germany). The prepared extract was kept in a sterilized bottle and stored at 4 °C [24].

2.2. Synthesis of Metal Nanoparticles

The green protocol was attempted for the synthesis of metal nanoparticle solutions using *P. undulata* plant extract following the method of Devasenan et al. [25]. About 1 mmol of metal slats, e.g., selenium sulfate, silver nitrate, and zinc sulfate, was well dissolved in 20 mL of deionized water. The salt solution in each case was gradually added to a stirred solution of the plant extract at 25 °C. The stirring process of the mixture was extended for an additional two hours until there was a notable change in the solution color. The absorbance of the solution was measured, together with the color intensity of the plant extract and the metal salt solution. The produced metal nanoparticle solution was kept in a dark bottle and stored in the refrigerator at 4 °C.

2.3. Characterization of Metal Nanoparticles

The physical properties and chemical structure, i.e., particle size, shape, surface nature, crystal structure, and morphological data of the prepared nanoparticles, were identified as conveyed by Otunola, et al. [26], using TEM (JEOL TEM-2100, Tokyo, Japan) at the Electron Microscope Unit, Mansoura University, Egypt. The analysis was run with a 200 nm magnification value. The optical properties of the zinc nanoparticles were studied using UV-VIS (Shimadzu UV-VIS 2450, Kyoto, Tapan) spectral analysis. FT-IR measurements were carried out using a Mattson-5000 FTIR spectrometer (Labexchange, Burladingen, Germany) in the range of 400–4000 cm^{-1} with a resolution of 8 cm^{-1} at room temperature.

The surface charge of the prepared zinc nanoparticles in the suspension was characterized by applying the zeta potential technique using Malvern Instruments Ltd. Zeta Potential Ver. 2.3 (Kassel, Germany), according to Bhattacharjee [27], at the Electron Microscope Unit, Mansoura University, Egypt. The process is significant for studying the surface nature of nanoparticles, and the stability of these particles can be expected to last for long periods [28].

2.4. Gas Chromatography-Mass Spectroscopic Analysis (GC-MS)

The volatile plant components of the extract were isolated and characterized efficiently using GC-MS spectrometry through the implementation of the Trace GC-TSQ mass spectrometer (Thermo Scientific, Austin, TX, USA) on the plant extract. The extracted components were interpreted based on the WILEY 09 and NIST 14 mass spectroscopic databases, relative to the obtained results.

2.5. Phytochemical Analysis

2.5.1. Total Tannin Contents

The amount of tannin was estimated via the vanillin–hydrochloride assay, based on the sample's absorbance after treatment with newly synthesized vanillin [29]. The extracted plant sample's tannin concentration was expressed as gram tannic acid equivalents/100-g dried plant. The samples' tannin capacity was determined from the tannic acid standard curve ($y = 0.0009\times$; $r^2 = 0.955$).

2.5.2. Total Phenolic Contents

The extracted plant material was tested for phenolics. The Folin-Ciocalteu (F-C) assay was performed according to Issa et al. [30], using the standard curve of Gallic acid to derive the characteristic values as milligram of Gallic acid equivalent/gram of dried plant. Gallic acid standard curves ($y = 0.0062\times$, $r^2 = 0.987$) were used.

2.5.3. Total Flavonoid Contents

Flavonoids are expressed as milligram catechin equivalent per gram of plant dry weight using the standard curve of standard catechin in aluminum chloride colorimetric testing for the extracted plant sample [31]. The standard curve ($y = 0.0028\times$, $r^2 = 0.988$) estimated the flavonoids.

2.6. Biological Procedures

2.6.1. Estimation of Antioxidant Activity

Kitts et al. assessed the antioxidant activity of the plant extract and metal nanoparticle solutions using the $DPPH^{\bullet}$ assay, using ascorbic acid as a reference [32]. In methanol, each sample was serially diluted. In the serial dilution, 0.135 mM $DPPH^{\bullet}$ solution was added to each sample. For 30 min, at 25 °C, the samples were stored in darkness. At 517 nm, samples were evaluated for color intensity absorption. The % remaining $DPPH^{\bullet}$ was obtained by stratifying the following equation:

$$\%\text{ remaining DPPH}^{\bullet} = [\text{DPPH}^{\bullet}]_T/[\text{DPPH}^{\bullet}]_{T=0} \times 100 \tag{1}$$

To determine the inhibitive concentration "IC_{50}, mg/mL", % remaining $DPPH^{\bullet}$ was plotted against the sample concentration using an exponential curve. IC_{50} values show a negative correlation with antioxidant ability [33].

2.6.2. Assessment of the Antibacterial Activity

Bacterial species: The various microbial species were obtained from the Faculty of Agriculture at Ain Shams University's Cairo Microbiological Resources Centre (Cairo MIRCEN, Cairo, Egypt). Gram-negative bacteria: *Escherichia coli* (ATKCC 105362), *Pseudomonas aeruginosa* (ATKCC 90278), *Salmonella typhimurium* (ATKCC 255661), and *Klebsiella pneumoniae* (ATKCC 100317). Gram-positive bacteria: *Bacillus cereus* (EMDCC number 108032), *Staphylococcus aureus* (ATKCC 65384), *Staphylococcus epidermidis* (ATKCC 12226), and *Bacillus subtilis* (DMAS 1088). Fungal species: *Candida albicans* (EMACC number 1053).

Microbial Testing: Agar well diffusion assays, with inoculate of 10^6 bacterial cells/mL dispersed over nutrient agar plates, were used to calculate the antibacterial activity of the plant extracts. Filter paper discs (Whatman no.1, 6 mm in diameter) were sterilized and soaked overnight in the plant extract until saturated. Filter paper discs were also immersed in methanol as a reference. The discs were then transferred to agar plates that had been pre-seeded with known strains of bacteria. After incubating the plates at 37 °C for 18–24 h, the diameters (mm) of the inhibitory zones were measured [34].

2.6.3. Cytotoxicity Assay

The HePG-2 (Hepatocellular carcinoma), MCF-7 (breast cancer), and PC3 (human prostate) were selected as human tumor cell lines, and WI-38 (fibroblasts derived from lung tissue) as the normal cell line were purchased from ATCC via a holding company for biological products and vaccines (VACSERA), Cairo, Egypt. To make the MTT solution, 10 mg/mL of MTT was dissolved in water, 20 mg/mL in ethanol, and 5 mg/mL in a buffered salt solution and medium. The components were combined using a vortex or sonication, filtered, and frozen at 20 °C.

For the MTT assay, the *P. undulata* extract and metal nanoparticle solutions were tested for cytotoxicity using an enhanced MTT colorimetric assay [35]. Each sample's IC_{50} was determined by seeding 3×10^3 cells/well in 100 µL of the complete medium onto 96-well plates. Seven culture medium concentrations were used to activate the cells. The plates were incubated in 5% CO_2 at 37 °C for 24 h to settle and adhere. After adhesion, the cells received a serial dilution of the samples for 48 h. Aspirating the medium, a weighed MTT (0.5 mg/mL) was dissolved in a culture-fresh solution and given to the cells. The plates were incubated at 37 °C and 5% CO_2 for 4 h. Each well received 100 µL SDS. At (λ_{max} = 570 nm) (BioTek, Elx800, Santa Clara, CA, USA), cell growth was reduced as a percentage of control. Origin 8.0® software (Origin Lab Corporation) was used to calculate the samples' IC_{50} values using the sigmoidal type of straight linear regression and using the fit line, Y = a*X + b, IC_{50} = (0.57 − b)/a. The percentage of cell growth inhibition was determined from Equation (2), where A is the absorbance read of the control and the tested sample:

$$\% \text{ Inhibition} = \frac{\text{A control} - \text{A sample}}{\text{A control}} \times 100 \tag{2}$$

The percentage of relative cell viability was determined using the following equation (Equation (3)), in which A represents the control and sample absorbance at λ_{max} = 570 nm. The results of this calculation were then used to determine the relative cell viability.

$$\% \text{ Cell viability} = \frac{\text{A treated samples} - \text{A blank}}{\text{A control} - \text{A blank}} \times 100 \tag{3}$$

3. Results and Discussion

The current work was intended to prepare and characterize metal nanoparticle solutions following the green protocol and using *P. undulata* extract as a natural source. The volatile components of the plant extract were characterized using GC-MS spectral analysis, and the metal nanoparticles were characterized using spectral and phytochemical analyses to estimate their biological profiles.

3.1. GC-MS Spectroscopy

The volatile components of methanol extract of *P. undulata* were determined using GC-MS analysis. The chromatogram in Figure 1 demonstrates the relative abundance of the detected volatile components concerning the retention times. The scan of the sample was run during 35.73 min of retention time. The results of the GC-MS analysis as shown in Table 1 indicated that twenty-five volatile components were recognized throughout the investigated retention time. Consequently, the most abundant component was interpreted for methyl oleate as a lipid or ester of the fatty acid type with 23.97% after 23.35 min.

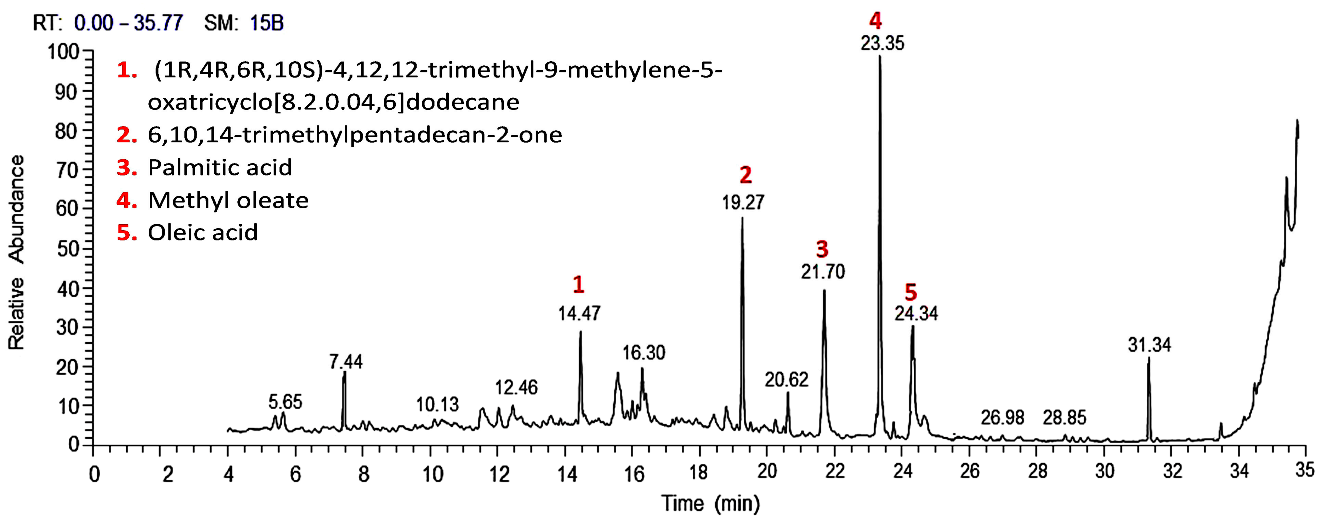

Figure 1. Chromatogram and structures of key volatile components of *P. undulata* extract derived via GC-MS.

Table 1. Chemical characterization of the components extracted from *P. undulata*.

Entry	Volatile Components	Classification	RT [a] (min)	M.Wt. [b]	M.Fw. [c]	Area (%)
			Hydrocarbons			
1	(2E,6E)-3,7-dimethylnona-2,6-dienal	Hydrocarbon	5.65	166.26	$C_{11}H_{18}O$	1.57
2	3,6-dimethyloctan-2-one	Hydrocarbon	7.44	156.27	$C_{10}H_{20}O$	1.53
3	(Z)-2-butylocta-2,7-dien-1-ol	Hydrocarbon	11.51	182.31	$C_{12}H_{22}O$	1.08
4	tetradeca-1,13-dien-3-one	Hydrocarbon	11.58	208.35	$C_{14}H_{24}O$	1.89
5	(1R,4R,6R,10S)-4,12,12-trimethyl-9-methylene-5-oxatricyclo[8.2.0.0^{4,6}]dodecane	Hydrocarbon	14.47	220.36	$C_{15}H_{24}O$	6.20
6	(1S,5R,9R)-10,10-dimethyl-2,6-dimethylenebicyclo[7.2.0]undecan-5-ol	Hydrocarbon	15.58	220.36	$C_{15}H_{24}O$	5.93
7	(2E,15Z)-14-methyloctadeca-2,15-dien-1-ol	Hydrocarbon	18.79	280.50	$C_{19}H_{36}O$	2.61
8	6,10,14-trimethylpentadecan-2-one	Hydrocarbon	19.27	268.49	$C_{18}H_{36}O$	12.77
9	Retinal "Vitamin A"	Hydrocarbon	20.25	284	$C_{20}H_{28}O$	1.03
10	3-ethyl-5-(2-ethylbutyl)octadecane	Hydrocarbon	33.47	366.72	$C_{26}H_{54}$	0.89
11	Heptatriacontan-1-ol	Hydrocarbon	35.73	537.01	$C_{37}H_{76}O$	2.69
			Fatty acids and esters			
12	Ethyl (9Z,12Z)-octadeca-9,12-dienoate	Ester of fatty acid	12.04	308.51	$C_{20}H_{36}O_2$	1.51
13	(Z)-7-methyltetradec-1-en-1-yl acetate	Ester of fatty acid	12.46	268.44	$C_{17}H_{32}O_2$	1.69
14	Methyl (5Z,8Z,11Z,14Z)-icosa-5,8,11,14-tetraenoate	Ester of fatty acid	16.29	318.50	$C_{21}H_{34}O_2$	3.33
15	Ethyl (9Z,12Z)-octadeca-9,12-dienoate	Ester of fatty acid	16.40	308.51	$C_{20}H_{36}O_2$	1.92
16	Methyl 14-methylpentadecanoate	Ester of fatty acid	20.62	270.46	$C_{17}H_{34}O_2$	2.75
17	Palmitic acid	Fatty acid	21.70	256.43	$C_{16}H_{32}O_2$	11.08
18	Methyl (7E,10E)-octadeca-7,10-dienoate	Ester of fatty acid	23.25	294.48	$C_{19}H_{34}O_2$	1.07
19	Methyl oleate	Ester of fatty acid	23.35	296.50	$C_{19}H_{36}O_2$	23.97
20	Methyl 16-methylheptadecanoate	Ester of fatty acid	23.76	298.51	$C_{19}H_{38}O_2$	1.08
21	Oleic acid	Fatty acid	24.33	282.47	$C_{18}H_{34}O_2$	4.25
22	(2-phenyl-1,3-dioxolan-4-yl)methyl (E)-octadec-9-enoate	Ester of fatty acid	35.25	444.66	$C_{28}H_{44}O_4$	1.26
23	2,2,8,8-tetramethyl-3,7-dioxa-2,8-disilanonan-5-yl oleate	Ester of fatty acid	35.41	500.91	$C_{27}H_{56}O_4Si_2$	5.56
			Terpenes			
24	(Z)-1-methyl-4-(6-methylhepta-2,5-dien-2-yl)-7-oxabicyclo[4.1.0]heptane	Sesquiterpene	16.01	220.36	$C_{15}H_{24}O$	1.31
			Steroids			
25	Stigmast-5-en-3-ol	Steroid	34.46	414.72	$C_{29}H_{50}O$	1.01
			Total			99.98

[a] RT: retention time, [b] M.Wt.: molecular weight, [c] M.Fw.: molecular formula.

The other extremely abundant molecules were interpreted as 6,10,14-trimethylpentadecan-2-one (12.77%) "hydrocarbon", palmitic acid (11.08%) "fatty acid", (1R,4R,6R,10S)-4,12,12-trimethyl-9-methylene-5-oxatricyclo[8.2.0.0^{4,6}]dodecane (6.20%), (1S,5R,9R)-10,10-dimethyl-2,6-dimethylene-bicyclo[7.2.0]undecan-5-ol (5.93%) "hydrocarbons", 2,2,8,8-tetramethyl-3,7-dioxa-2,8-disilanonan-5-yl oleate (5.56%), oleic acid (4.25%) "fatty acid", and methyl (5Z,8Z,11Z,14Z)-icosa-5,8,11,14-tetraenoate (3.33%) "lipid". The majority of these components are related to fatty acids or esters of fatty acids or oxygenated hydrocarbons. The other components were found to be rare or abundant, with composition percentages ranging from 0.89 to 2.75%.

The inferred data of the investigated volatile components were classified into two main categories identified as hydrocarbons, fatty acids, and esters of fatty acids, along with rare percentages for terpenes (1.31%) and steroids (1.01%) (Table 1). The category of fatty acids and esters of fatty acids is the major class of components, with a total of 59.47%, whereas hydrocarbons made up 38.19%. Twelve components were categorized as fatty acids and esters of the fatty acid class, with the most abundant molecule identified as methyl oleate (23.97%). Hydrocarbons comprised eleven components, with the major area percentage for 6,10,14-trimethylpentadecan-2-one (12.77%).

Additionally, one component for each of the terpenes and steroids documented were recorded as (*Z*)-1-methyl-4-(6-methylhepta-2,5-dien-2-yl)-7-oxabicyclo[4.1.0]heptane, and stigmast-5-en-3-ol, respectively. Many studies, such as those reported by Abdallah et al. [36] and Al-Hajj et al. [37], investigated the characterization of the volatile components of the extracted *P. undulata*, including the characterization of long-chain fatty acids. The volatile components of the petroleum ether extract of the whole plant of *P. undulata* were characterized using GC-MS spectroscopy analysis, as investigated by Elshiekh and Mona [14]. Furthermore, Mansour [38] specified the volatile components of *P. undulata*, signifying methyl linoleate (18.84%) as a fatty acid derivative.

3.2. Characterization of the Metal/Metal Oxide Nanoparticles

3.2.1. Transmission Electron Microscope (TEM)

TEM analysis was used to define the nature and crystallography of the nanoparticles prepared using *P. undulata* plant extract, for instance, particle size, shape, and aggregation, as conveyed by Otunola et al. [26]. The analyses of the samples were run on TEM (JEOL TEM-2100) with 200 nm of magnification at the Electron Microscope Unit, Central Laboratory, Mansoura University. Figure 2 presents the TEM charts of the prepared nanoparticles of silver, selenium, and zinc. Given the nanoparticle size, it is worth mentioning that in all cases of the three solutions of silver, selenium, and zinc nanoparticles the recorded data referred to a reduced size of less than 100 nm. The particle size in the case of selenium nanoparticles was recorded at 78.16, and 89.64 nm. The nanoparticles in the cases of silver and selenium solutions have spherical shapes, while in the case of zinc, it is noted as having spherical, trigonal, and tetragonal shapes. Whatever the shape, the spherical shapes provided the largest surface area, with improved influence from the impact of the biological solution. In addition, the nanoparticles are more aggregated in the case of the silver solution, followed by the zinc and selenium solutions. The aggregation factor controlled the efficiency of the solution with respect to improved biological results.

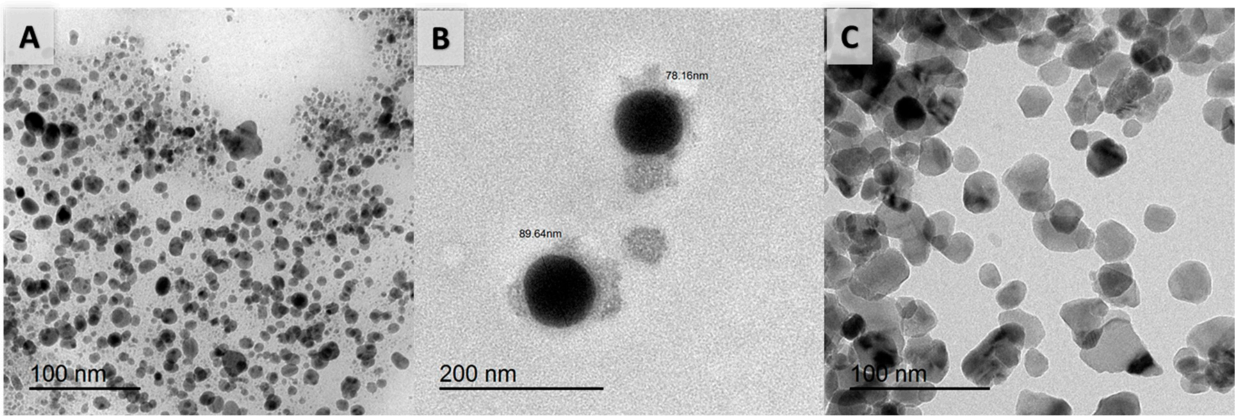

Figure 2. TEM configurations of (**A**) AgNPs, (**B**) SeNPs, and (**C**) ZnNPs.

3.2.2. Zeta Potential Analysis

Zeta potential analyses (Figure 3) were run for the prepared metal nanoparticles using *P. undulata* plant extract to investigate the surface charge in suspension, using Malvern Instruments Ltd. Zeta Potential Ver. 2.3, as in Bhattacharjee [27].

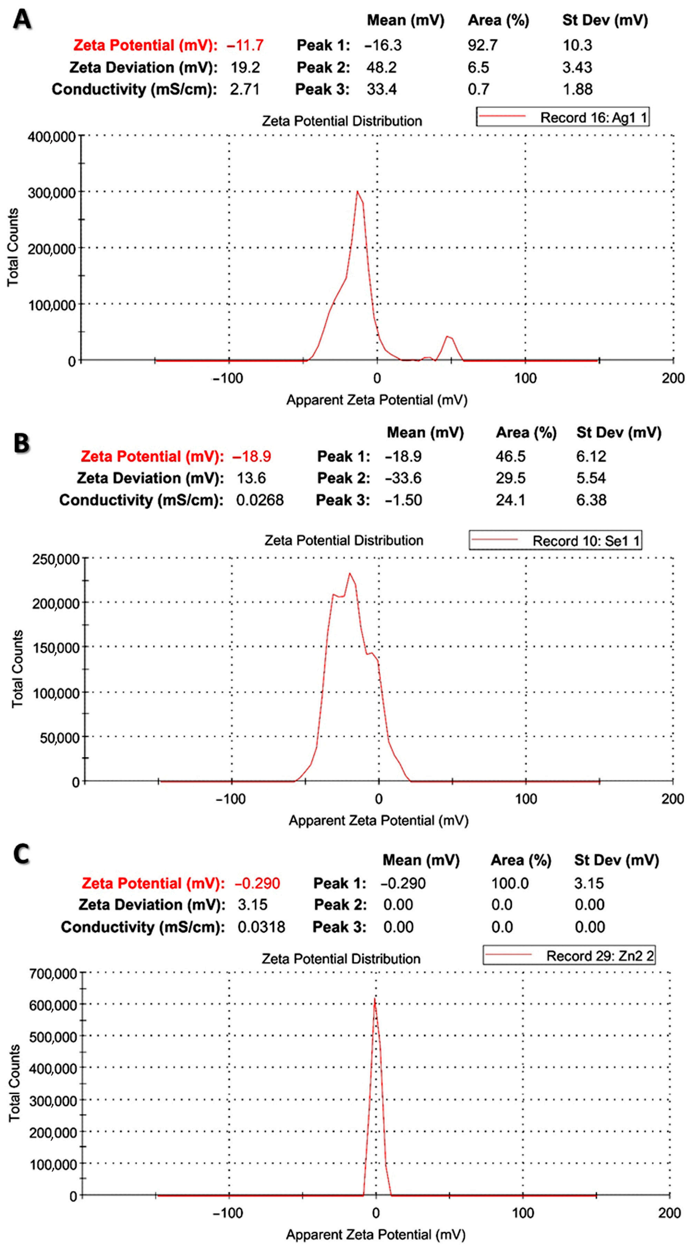

Figure 3. Zeta potential analysis of (**A**) AgNPs, (**B**) SeNPs, and (**C**) ZnNPs.

The process is a noteworthy device for examining the surface state of the nanoparticle, and imagines the long-term stability of the metal nanoparticle. The native surface charge of the nanoparticles might attract a thin layer of ions with opposite charges.

Zeta potential performance (Figure 3) was useful for identifying the surface charge. Nanoparticles have a double layer of ions, which move as they disperse in the solution; the electric potential at the border of the double layer is documented as the zeta potential of the particles and has typical values in the range of +100 mV to −100 mV. The synthesized silver, selenium, and zinc nanoparticles using *P. undulata* extract have zeta potential values of −11.7, −18.9, and −0.290 mV, which showed high stability owing to nanoparticles with zeta potential values of less than +25 mV or higher than −25 mV representative of high stability degrees, as stated by Honary and Zahir [28].

3.2.3. UV–Visible Spectrophotometer

The synthesized ZnO-NPs, SeO_2-NPs, and AgNPs solutions were analyzed for their optical properties using a UV-Vis spectrophotometer with a scan range from 190.00 to 1090.0 nm. The results specified that the maximum absorbance reads of ZnO-NPs, SeO_2-NPs, and AgNPs were recorded at 246.0 nm; this indicated the formation of the respective nanoparticles in the solution, and it was confirmed as a sign of this, as shown in Figure 4. The maximum absorption peak was recorded for the *P. undulata* plant extract at a wavelength of 470 nm with absorbance at 0.893. The blue shift of the absorption spectra of the tested ZnO-NPs, SeO_2-NPs, and AgNPs solutions was noted. This behavior is in agreement with previous studies [39] and depends on the sample concentration, energy, light speed, and wavelength. The data confirmed clearly that zinc, selenium, and silver ions are proficiently reduced by the extract of *P. undulata*.

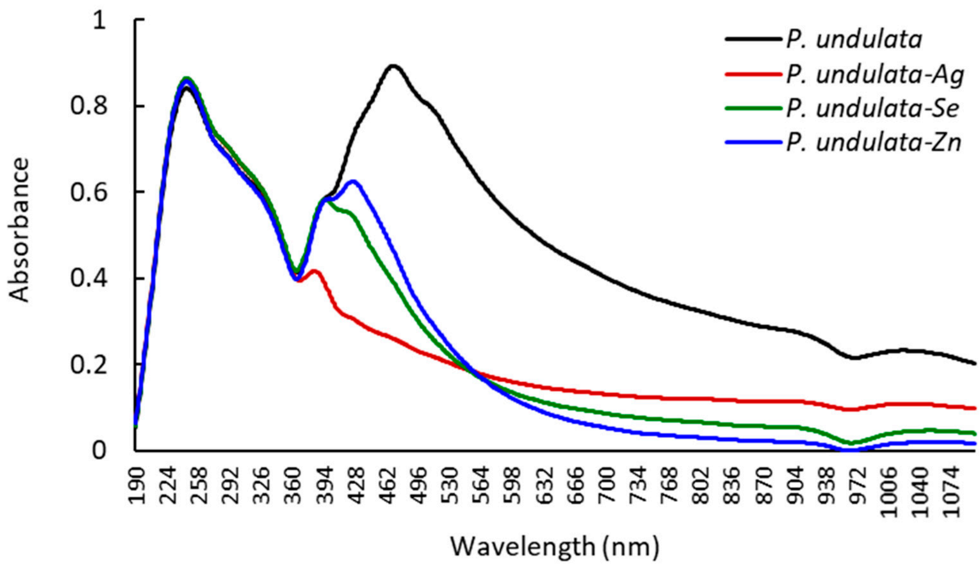

Figure 4. The UV-visible spectroscopy graphs of the prepared silver, selenium, and zinc nanoparticles.

3.2.4. FT-IR Measurements

The FT-IR spectrum analyses were run at Thermo-Fisher Nicolet IS10, USA Spectrophotometer. Fourier-transform infrared spectroscopy (FT-IR) was used to establish the characteristic functional groups of the tested samples. A simultaneous collection of high-resolution spectral data was inspected over a wide spectral range. The scale range of frequency in the range of ν = 4000 to 500 cm^{-1} was plotted against the transmittance percentages. The analysis of FT-IR was utilized to identify the characteristic functional groups of all samples. The formation of the respective nanoparticles of metal/and or metal oxide nanoparticles was well known through the disappearance of some functional groups in the FT-IR analysis, along with the shift of other groups in their frequencies.

The Figures S1–S4, and Table 2 present the FT-IR spectroscopic data of *P. undulata*, and its metal/metal oxide nanoparticles, for example, silver, selenium dioxide, and zinc oxide nanoparticles. Accordingly, all the samples revealed the presence of absorption bands at ν = 3414–3420 cm^{-1}, in which these absorption bands are attributed to the vibrations of sharp O-H stretching groups, indicating the presence of alcoholic groups.

Table 2. The characteristic FT-IR data and functional groups of *P. undulata* extract, and its metal/metal oxides nanoparticles.

P. undulata Extract	Ag NPs	SeO_2 NPs	ZnO NPs	Appearance	Functional Group
3414	3420 *	3420	3418	Sharp	O-H stretching
2933	2931	2927	-	Medium	C-H stretching
1619	1620	1628	1628	Weak, Strong	C-O stretching
1387	1385	1385	1402	Medium	C-H bending
1270	1263	-	1283	Medium	C-O-H
1037	1077	1050	1082	Medium	C-N stretching
601	602	605	693	Strong	C-H bending

* Absorption (cm^{-1}).

In addition, medium absorption bands were recorded for the C-H stretching group in the analysis of *P. undulata*, silver, and selenium dioxide nanoparticles at ν = 2927–2933 cm^{-1}, along with the disappearance of this band in the analysis of zinc oxide nanoparticles. This indicated that the interaction of a definite functional group with the metal ions in the solution or this functional group was reduced in the process of the formation of the metal/metal oxide nanoparticles. Our findings match with the literature reports regarding the disappearance of the absorption bands related to the C-H stretching group. Specifically, an absorption band was attributed to weak and strong C-O stretching or amidic carbonyl at ν = 1619–1628 cm^{-1} in the FT-IR analysis of all samples "*P. undulata*, and its metal/metal oxides nanoparticles"; this was perceived in the recorded shifts of these groups. The splitting/shifting of CO vibrational bands has been previously reported by Zeinalipour-Yazdi et al. [40], through the formation of metal nanoparticles. Correspondingly, a medium absorption band at ν = 1387 cm^{-1} is attributed to the C-H bending frequency in the analysis of the *P. undulata* extract, while the analyses of metal/metal oxides nanoparticles revealed shifts in the same range of frequency (ν = 1385–1402 cm^{-1}). These findings have established the vibrations of aliphatic chain moieties in the structure of the extracted components. The absorption bands at these ranges demonstrated the presence of alkane chains of the sp^3 C-H bond. The absorption bands that are attributed to medium C-O-H at a range of ν = 1263–1283 cm^{-1} were recorded in the analysis of *P. undulata* and its silver and zinc oxide nanoparticles, while this absorption band disappeared in the analysis of selenium dioxide nanoparticles. Precisely, the absorption bands at ν = 1037–1082 cm^{-1} in the analysis of *P. undulata*, and its metal/metal oxides nanoparticles are attributed to the presence of medium C-N stretching groups. Strong absorption bands appeared at ν = 602–693 cm^{-1}, specifying the presence of C-H binding vibrations. In general, the shift in these values confirmed the participation of this group in the formation of metal/metal oxide nanoparticles [19].

3.3. Phytochemical Analysis

The phytochemical analyses of factors such as the phenolic, flavonoid, and tannin contents of the extracted *P. undulata* and the solutions of metal nanoparticles were evaluated using quantitative methods. Generally, the phenolic contents located in the majority of the components were relative to the notable values of flavonoids and tannins. The results shown in Figure 5 indicate that the *P. undulata* extract has the highest values of phenolics (287.7446 mg gallic acid/1 gm dry extract), flavonoids (99.28444 mg catechine/1 gm dry extract), and tannins (24.4832 mg tannic acid/1 gm dry extract), relative to the metal nanoparticle solutions. This behavior is in agreement with the literature, since the phenolic components are responsible for the transformation of metal ions into metal oxide nanoparticles [41].

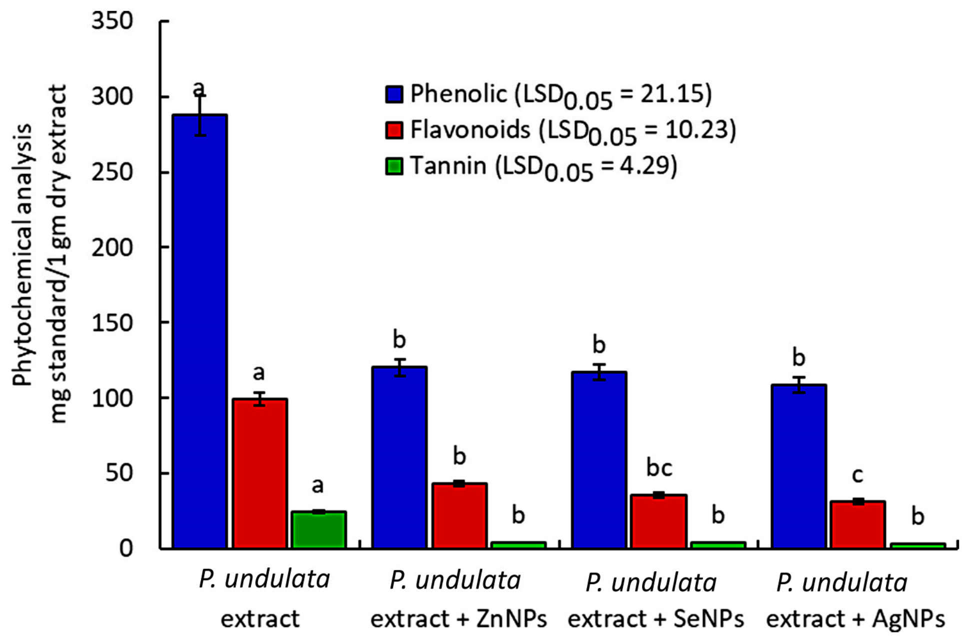

Figure 5. Phytochemicals of *P. undulata* extract and their various nanoparticles. Different letter for each bioactive group's mean value of significance at probability level of 0.05.

The phytochemical components participated in the oxidation process of the metal ions into the respective oxides, and thus the phytochemical components in the case of metal nanoparticle solutions were recorded with reduced values when compared to the original plant extract. In this context, ZnNPs recorded the greatest value of phenolic content (120.1557 mg gallic acid/1 gm dry extract) relative to the values of phenolic content of SeNPs and AgNPs. The same behavior was noted regarding the flavonoid content (43.15433 mg catechine/1 gm dry extract) in comparison to the SeNPs and AgNPs (35.38238, and 31.3781 mg catechine/1 gm dry extract). Also, there was a remarkable decrease in the values of tannin content when compared to the extracted *P. undulata* in the case of metal nanoparticle solutions in the range of 4.025157 to 3.29582 mg tannic acid/1 gm dry extract.

3.4. Biological Evaluation

3.4.1. DPPH Antioxidant Activity

The DPPH$^{\bullet}$ free radical test was used to measure the extract and metal nanoparticles of *P. undulata* for their potential antioxidant scavenging activities. The antioxidant capacity is the ability of the sample to trap DPPH free radicals in the solution in a free radical mechanism (Table 3). The comparison of the results of the tested samples with that of ascorbic acid verified that the plant extract shows better activity for trapping the free radicals of DPPH in the solution than the metal nanoparticle solutions. The results, in general, agree with the phytochemical results, as the phenolic contents enable a better efficiency of the sample in trapping the free radicals in the solution.

Table 3. The antioxidant results (% remaining DPPH, and % scavenging activity) of the metal nanoparticle solutions prepared with the extracted *P. undulata*.

Sample	Concentrations (mg/mL)	Scavenging Activity (%)
P. undulata extract	0.034	61.95 ± 2.82 ^{A}
	0.017	36.92 ± 1.68 ^{B}
	0.008	16.55 ± 0.75 ^{C}
	0.004	11.03 ± 0.50 ^{D}
	IC_{50}	0.025
	LSD	2.83 ***
	F-value	706.94

Table 3. *Cont.*

Sample	Concentrations (mg/mL)	Scavenging Activity (%)
P. undulata extract + ZnNPs	0.207	83.81 ± 3.81 [A]
	0.104	73.11 ± 3.32 [B]
	0.052	42.04 ± 1.91 [C]
	0.026	24.93 ± 1.13 [D]
	IC_{50}	0.062
	LSD	4.18 ***
	F-value	452.18
P. undulata extract + SeNPs	0.358	85.38 ± 3.88 [A]
	0.179	57.05 ± 2.59 [B]
	0.089	38.64 ± 1.76 [C]
	0.045	31.85 ± 1.45 [D]
	IC_{50}	0.125
	LSD	3.95 ***
	F-value	390.28
P. undulata extract + AgNPs	0.122	71.72 ± 3.26 [A]
	0.061	48.79 ± 2.22 [B]
	0.031	19.84 ± 0.90 [C]
	0.015	13.67 ± 0.62 [D]
	IC_{50}	0.068
	LSD	3.02 ***
	F-value	846.81
Zinc-Ascorbic acid	0.013	54.56 ± 2.48 [A]
	0.007	27.75 ± 1.26 [B]
	0.003	13.4 ± 0.61 [C]
	0.002	2.681 ± 0.12 [D]
	IC_{50}	0.012
	LSD	2.54 ***
	F-value	828.21
Ascorbic acid	0.062	85.19 ± 3.87 [A]
	0.031	62.07 ± 2.82 [B]
	0.016	40.74 ± 1.85 [C]
	0.008	27.41 ± 1.25 [D]
	IC_{50}	0.0222
	LSD	4.96 ***
	F-value	276.55

Different letter for each treatments mean value of significance at probability level of 0.05. *** $p < 0.001$.

The extracted *P. undulata* recorded 61.95% of the total percentage scavenging activity at a concentration of 0.034 mg/mL; this result is comparable to that of ascorbic acid (85.19% at 0.062 mg/mL). Although the results of scavenging activity percentages of the prepared ZnNP (83.81%), SeNP (85.38%), and AgNP (71.72%) solutions appeared to be higher than that of the plant extract itself, or in some cases higher than the ascorbic acid, these values were recorded at higher concentrations of these solutions. Several *Pulicaria* species extracts have been investigated and seen to possess considerable antioxidant activities, including *P. undulata* [12,13], *P. somalensis* [42], *P. inuloides* [37], and *P. vulgaris* [43].

The results of IC_{50} values (Table 3) indicated a noteworthy antioxidant capacity of the samples tested with IC_{50} = 0.025–0.125 mg/mL, relative to the result for ascorbic acid (IC_{50} = 0.0222 mg/mL). Accordingly, the zinc–ascorbic acid mixture (IC_{50} = 0.012 mg/mL) revealed improved potency when compared to the ascorbic acid solution. The most potent antioxidant capacity was recorded for the extracted *P. undulata*, with an IC_{50} value of 0.025 mg/mL. The formation of the metal nanoparticles (e.g., ZnNPs, SeNPs, and AgNPs) by the action of the *P. undulata* extract resulted clearly in the reduction in the antioxidant scavenging activity. As a result, the ZnNP solution revealed potent antioxidant capacity, with an IC_{50} value of 0.062 mg/mL, a better antioxidant capacity than either AgNP (IC_{50} = 0.068 mg/mL) or SeNP (IC_{50} = 0.125 mg/mL) solutions. The mechanism of this antioxidant process involved the accessibility of oxygen sources such as oxygenated hydrocarbons, fatty acids, phenolic components, and esters of fatty acids to trap the free radicals of DPPH in the solution. The major volatile components of this plant extract are found to be methyl oleate, palmitic acid, and 6,10,14-trimethylpentadecan-2-one, which have the possibility of terminating the free radical reactions [44,45].

3.4.2. Cytotoxic Activity

The cytotoxic activity was assessed for the extracted *P. undulata* and its ZnO-NP, SeO_2-NP, and AgNP solutions by applying MTT assay against the different tumor and normal cell lines. The results (Figure 6) showed improved cytotoxicity of the metal nanoparticle solutions when compared to the plant extract, in general, against the tumor cell lines. In particular, the SeO_2-NP solution prepared using the *P. undulata* extract is the most potent cytotoxic agent against the HePG-2 cell line, with an IC_{50} value of 9.20 mg/mL relative to the behavior of the extracted *P. undulata* (IC_{50} = 49.285 mg/mL). The potency of the selenium dioxide nanoparticle solution is comparable to the standard doxorubicin (IC_{50} = 6.026 mg/mL), with very strong potency against the HePG-2 cell line. Also, the silver nanoparticle solution revealed strong cytotoxic potency against the MCF-7 cell line (IC_{50} = 18.4 mg/mL) and moderate activity against the PC3 cell line (IC_{50} = 30.387 mg/mL).

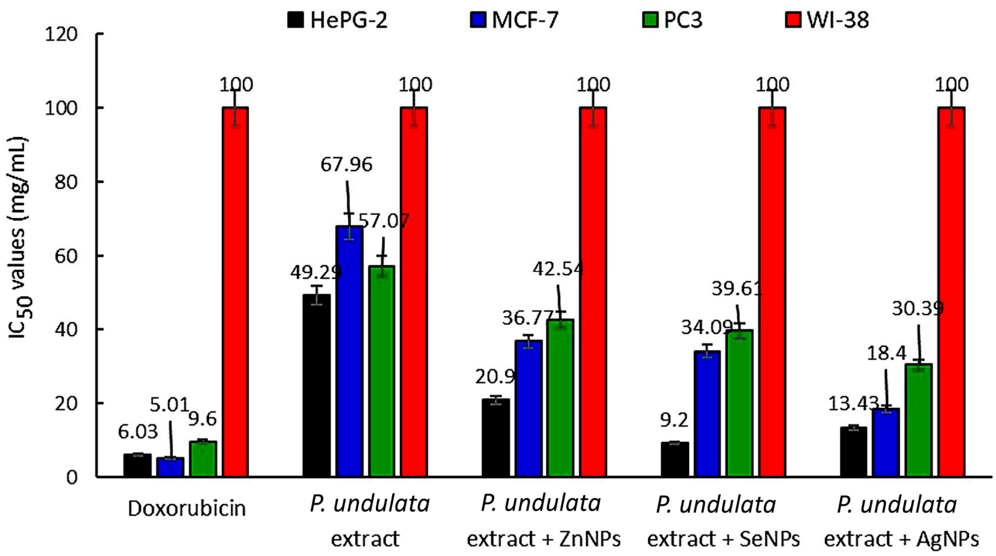

Figure 6. Cytotoxic activity of *P. undulata* extracts and their various nanoparticles, as well as the standard doxorubicin.

On the other hand, the *P. undulata* extract is more reliable and active against the growth of the HePG-2 cell line (IC_{50} = 49.285 mg/mL) in comparison to its activity against the other tumor cells. The same behavior was noticed for all metal oxide nanoparticle and silver nanoparticle solutions against the inhibition of cancer cell growth of the type HePG-2. The plant extract and metal nanoparticles revealed no activity against the growth of the normal cell line (WI-38) with IC_{50} values higher than 100 mg/mL. The remarkable cytotoxic performance of the metal nanoparticle solutions against the growth of tumor cell lines when compared to the plant extract is in agreement with the literature reports [46,47].

Moreover, the percentages of inhibition were calculated at seven concentrations (1.56–100 mg/mL) against all tumor and normal cells (Table 4). The results specified notable percentages of inhibitions at the higher concentrations. Thus, at the concentration of 100 mg/mL, *P. undulata* extract revealed good cytotoxic potency against HePG-2, MCF-7, and PC3 tumor cells, with % inhibitions at 64.5, 56.7, and 64.5%, respectively. The results are accompanied by reduced inhibition against the WI-38 normal cell line, with 9.22% of inhibition. The silver nanoparticle solution revealed the most potent percentage of inhibition at 85.6% against HePG-2 tumor cells at the higher concentration (100 mg/mL).

Table 4. The percentages of inhibition at different concentrations against the studied tumor and normal cell lines.

Samples	Conc. (mg/mL)	% Inhibition			
		HePG-2	MCF-7	PC3	WI-38
Doxorubicin	100	94.20	94.31	92.4	10.11
	50	89.51	90.21	82.6	8.75
	25	86.32	86.10	76.3	6.55
	12.5	69.50	74.70	59.2	3.78
	6.25	52.33	56.91	42.7	1.87
	3.125	40.10	41.62	26.4	0.67
	1.56	26.6	28.51	23.9	0.02
P. undulata extract	100	64.5	56.70	64.5	9.22
	50	54.13	45.40	50.3	7.70
	25	42.45	35.31	38.1	5.66
	12.5	31.43	24.10	28.4	3.50
	6.25	20.15	18.60	21.3	1.65
	3.125	9.47	11.32	17.9	0.33
	1.56	5.72	8.74	9.34	0.00
P. undulata extract + ZnNPs	100	72.54	66.65	64.9	10.12
	50	63.04	56.91	54.2	9.70
	25	56.14	46.04	40.3	7.55
	12.5	45.89	33.33	32.8	6.50
	6.25	36.08	16.06	24.6	5.74
	3.125	24.11	20.66	21.64	3.33
	1.56	2.12	0.00	0.00	2.88
P. undulata extract + SeNPs	100	80.32	69.3	66.07	12.12
	50	70.16	61.14	57.03	10.57
	25	64.34	52.01	47.86	8.35
	12.5	50.60	40.77	40.33	7.85
	6.25	40.20	28.16	30.55	5.63
	3.125	27.40	11.56	9.34	3.34
	1.56	10.81	3.22	1.35	1.82
P. undulata extract + AgNPs	100	85.6	76.90	74.11	8.40
	50	76.73	70.10	63.20	6.80
	25	66.98	57.34	56.01	5.16
	12.5	53.5	46.87	44.7	4.56
	6.25	30.44	31.80	34.1	3.24
	3.125	24.61	22.94	27.09	2.45
	1.56	10.65	11.09	13.76	1.82

The cytotoxic mechanism is affected by several factors, which can be concluded to be the sample concentration, the nature of the extracted components, phytochemical contents, properties of the nanoparticles such as shape, size, and aggregation, the type of tumor and normal cell line, and cytotoxicity associated with the loss of cell protein [20,48,49].

3.4.3. Antimicrobial Activity

The antimicrobial activity of the extracted *P. undulata*, and its metal nanoparticle solutions against various gram-positive, and negative bacterial species and the pathogenic yeast *C. albicans* fungal species was assessed using a disc diffusion assay. The results (Table 5) specified no activity of the extracted plant against all the tested microbial species. In addition, the solutions of the synthesized nanoparticles revealed a broad spectrum of antimicrobial activity against the diverse microbial species. These results agree with that obtained by Shirzadi-Ahodashti et al. [50] on the extracted *Crataegus monogyna* leaf, relative to the results developed from the silver and gold nanoparticles prepared from this extract.

Table 5. The antimicrobial activity of *P. undulata* extract and its nanoparticles against varieties of microbial species.

Microbial Species	*P. undulata* Extract (50 µg/Disk)		*P. undulata* Extract ± NPs (µg mL^{-1})					
			SeNPs		ZnNPs		AgNPs	
	IZ [a]	MIC [b]	IZ	MIC	IZ	MIC	IZ	MIC
			Gram-negative species					
Escherichia coli	ND [c]	0.0	38.3 ± 0.93 ^{A}	9	18.81 ± 0.44 ^{ABC}	10	13.72 ± 0.32 ^{A}	11
Salmonella typhi	ND	0.0	20.16 ± 0.49 ^{C}	11	20.32 ± 0.50 ^{A}	9	12.61 ± 0.29 ^{AB}	14
Pseudomonas aeruginosa	ND	0.0	14.23 ± 0.34 ^{D}	12	15.91 ± 0.37 ^{D}	11	12.34 ± 0.30 ^{AB}	15
Klebsiella pneumonia	ND	0.0	21.72 ± 0.51 ^{BC}	10	20.58 ± 0.49 ^{A}	9	12.55 ± 0.29 ^{AB}	15
			Gram-positive species					
Bacillus cereus	ND	0.0	23.08 ± 0.56 ^{BC}	10	17.47 ± 0.41 ^{BCD}	8	13.48 ± 0.32 ^{A}	12
Staphylococcus aureus	ND	0.0	13.39 ± 0.32 ^{D}	14	16.34 ± 0.39 ^{CD}	8	12.67 ± 0.31 ^{A}	15
Bacillus subtilis	ND	0.0	22.07 ± 0.54 ^{BC}	10	19.27 ± 0.46 ^{AB}	9	9.35 ± 0.22 ^{C}	25
Staphylococcus epidermidis	ND	0.0	24.16 ± 0.59 ^{B}	9	15.18 ± 0.37 ^{D}	11	11.48 ± 0.24 ^{B}	16
			Pathogenic yeast					
Candida albicans	ND	0.0	21.05 ± 0.51 ^{BC}	11	0.00 ^{E}	-	11.09 ± 0.27 ^{B}	17
$LSD_{0.05}$			3.08 ***		2.31 ***		1.38 ***	

[a] IZ: inhibition zone (mm) ± standard error, [b] MIC: minimum inhibitory concentration, [c] ND: refers to the undetected values, the "inactive antimicrobial agent". Different superscript letters for each group of organisms and treatments mean value significance at probability level of 0.05. *** $p < 0.001$.

In particular, the selenium nanoparticles revealed the most potent activity against *E. coli* (inhibition zone diameter = 38.3 mm), *K. pneumonia* (21 mm), *B. cereus* (23 mm), *B. subtilis* (22 mm), *S. epidermidis* (24 mm) bacterial strains, and *C. albicans* (21 mm) fungal strains. In addition, ZnNPs displayed the most potent activity against *S. Typhi* (20.3 mm), *P. aeruginosa* (15 mm), and *S. aureus* (16 mm) bacterial strains. These results supported the high potency of the SeNP solution against most of the microbial species when compared to ZnNPs, and AgNPs, but the efficiency of all solutions to inhibit the growth of microbial species is still noted. The SeNPs have been reported to possess substantial in vitro and in vivo biological activities, as well as low toxicity at the same time [51–53]. These results agree with that recently obtained by Vinu et al. [54] for *Vibrio parahaemolyticus*, as well as El-Amier et al. [2] and El-Zayat et al. [55] for *Ephedra aphylla* and *Senecio glaucus* extract against a diversity of microbial species. On the other hand, it was noted that the SeNP solution recorded the highest antimicrobial potency against *E. coli* (mm), while the ZnNP solution displayed the most potent activity against *S. Typhi* (20.3 mm), along with the remarkable potency of the AgNP solution against *E. coli*, and *B. cereus* species (38.3 mm).

Based on the IC_{50}, the SeNPs generated by the *P. undulata* extract showed the lowest IC_{50} value (9 µg mL^{-1}) against *E. coli*, while showing IC_{50} values of 10, 11, and 12 µg mL^{-1} against *K. pneumonia*, *S. typhi*, and *P. aeruginosa*, respectively (Table 5). On the other hand, the ZnNP solution showed post antimicrobial activity against *S. typhi* and *K. pneumonia*, where it attained an IC_{50} value of 9 µg mL^{-1}, while the AgNP solution showed the lowest IC_{50} value (11 µg mL^{-1}) and the highest IC_{50} value (15 µg mL^{-1}) against *P. aeruginosa* and *K. pneumonia*, respectively (Table 5).

To discuss the mechanism of action of these behaviors, it was mandatory to study the susceptibility and resistance of bacterial species, and the tolerance, persistence, sample concentration, and host response [56]. The nanoparticle size, shape, and aggregation factors also affected the antimicrobial potency, with significant results [57]. On the other hand, the main volatile components that were interpreted using GC-MS spectrometry were utilized in the formation of metal oxide nanoparticles such as zinc oxide and selenium dioxide, with the reduction in the functional groups of these components. In particular, the methyl oleate, palmitic acid, and 6,10,14-trimethylpentadecan-2-one components that were characterized using the *Reichardia tingitana* and *Alnus nitida* extracts were reported to have privileged biological potency in terms of antimicrobial, antioxidant, and cytotoxic activities, as reported by Salama, et al. [45], and Shaukat, et al. [58].

4. Conclusions

In this work, *P. undulata* extract was employed for the green synthesis of metal nanoparticles such as selenium, zinc, and silver nanoparticles. The mechanism of this process is related to the utility of the active components in the plant extract for oxidizing the metal ions or transforming these ions into zero states with the formation of metal oxides in the solution on a nano-size scale. The process involved the formation of zinc oxide and selenium dioxide nanoparticles, along with the formation of silver nanoparticles in the zero-state. In this section, the characterization of the chemical profile was investigated using GC-MS spectroscopy and estimation of the phytochemical contents was carried out. The formation of metal nanoparticles was tested using TEM, zeta potential, and UV-visible spectra. The biological potency of the plant extract and its metal nanoparticles revealed the decreased antioxidant characteristics of the original extract of this plant, along with improved cytotoxicity, and antimicrobial characteristics. Thus, using an eco-friendly protocol, such as green synthesis, for the formulation of nanomaterials is considered an efficient tool, and the produced nanomaterials have shown a cytotoxic and antimicrobial potentiality that could be included in developing pharmaceutical studies on a large scale.

Supplementary Materials: The following supporting information can be downloaded at: https://www.mdpi.com/article/10.3390/chemistry5040141/s1, Figure S1: The FT-IR spectral chart of *P. undulata* extract; Figure S2: The FT-IR spectral chart of *P. undulata* extract -Ag NPs; Figure S3: The FT-IR spectral chart of *P. undulata* extract -SeO2 NPs; Figure S4: The FT-IR spectral chart of *P. undulata* extract -ZnO NPs.

Author Contributions: Conceptualization, Y.A.E.-A. and M.M.E.-Z.; formal analysis, Y.A.E.-A., B.T.A. and M.M.E.-Z.; investigation, Y.A.E.-A., B.T.A., M.M.E.-Z., T.C.S. and A.M.A.-E.; writing—original draft preparation, Y.A.E.-A. and A.M.A.-E.; writing—review and editing, Y.A.E.-A., B.T.A., M.M.E.-Z., T.C.S. and A.M.A.-E. All authors have read and agreed to the published version of the manuscript.

Funding: This research was supported by The Researchers Supporting Project number (RSPD2023R676) King Saud University, Riyadh, Saudi Arabia.

Data Availability Statement: Not applicable.

Acknowledgments: The authors extend their appreciation to The Researchers Supporting Project number (RSPD2023R676) King Saud University, Riyadh, Saudi Arabia.

Conflicts of Interest: The authors declare no conflict of interest.

References

1. Elshamy, A.I.; Farrag, A.R.H.; Ayoub, I.M.; Mahdy, K.A.; Taher, R.F.; Gendy, A.E.-N.G.E.; Mohamed, T.A.; Al-Rejaie, S.S.; Ei-Amier, Y.A.; Abd-EIGawad, A.M. UPLC-qTOF-MS phytochemical profile and antiulcer potential of *Cyperus conglomeratus* Rottb. alcoholic extract. *Molecules* **2020**, *25*, 4234. [CrossRef] [PubMed]
2. El-Amier, Y.; Abdelghany, A.; Abed Zaid, A. Green synthesis and antimicrobial activity of *Senecio glaucus*-mediated silver nanoparticles. *Res. J. Pharm. Biol. Chem. Sci.* **2014**, *5*, 631–642.
3. Boukhatem, M.N.; Setzer, W.N. Aromatic herbs, medicinal plant-derived essential oils, and phytochemical extracts as potential therapies for coronaviruses: Future perspectives. *Plants* **2020**, *9*, 800. [CrossRef] [PubMed]
4. Mohammed, A.B.; Yagi, S.; Tzanova, T.; Schohn, H.; Abdelgadir, H.; Stefanucci, A.; Mollica, A.; Mahomoodally, M.F.; Adlan, T.A.; Zengin, G. Chemical profile, antiproliferative, antioxidant and enzyme inhibition activities of *Ocimum basilicum* L. and *Pulicaria undulata* (L.) CA Mey. grown in Sudan. *South Afr. J. Bot.* **2020**, *132*, 403–409. [CrossRef]
5. Al-hamoud, K.; Shaik, M.R.; Khan, M.; Alkhathlan, H.Z.; Adil, S.F.; Kuniyil, M.; Assal, M.E.; Al-Warthan, A.; Siddiqui, M.R.H.; Tahir, M.N.; et al. *Pulicaria undulata* extract-mediated eco-friendly preparation of TiO_2 nanoparticles for photocatalytic degradation of methylene blue and methyl orange. *ACS Omega* **2022**, *7*, 4812–4820. [CrossRef]
6. Mustafa, A.M.; Eldahmy, S.I.; Caprioli, G.; Bramucci, M.; Quassinti, L.; Lupidi, G.; Beghelli, D.; Vittori, S.; Maggi, F. Chemical composition and biological activities of the essential oil from *Pulicaria undulata* (L.) CA Mey. Growing wild in Egypt. *Nat. Prod. Res.* **2020**, *34*, 2358–2362. [CrossRef]

7. Abd-ELGawad, A.M.; Al-Rowaily, S.L.; Assaeed, A.M.; Ei-Amier, Y.A.; El Gendy, A.E.-N.G.; Omer, E.; Al-Dosari, D.H.; Bonanomi, G.; Kassem, H.S.; Elshamy, A.I. Comparative chemical profiles and phytotoxic activity of essential oils of two ecospecies of *Pulicaria undulata* (L.) CA Mey. *Plants* **2021**, *10*, 2366. [CrossRef]
8. Ali, N.A.A.; Sharopov, F.S.; Alhaj, M.; Hill, G.M.; Porzel, A.; Arnold, N.; Setzer, W.N.; Schmidt, J.; Wessjohann, L. Chemical composition and biological activity of essential oil from *Pulicaria undulata* from Yemen. *Nat. Prod. Commun.* **2012**, *7*, 257–260. [CrossRef]
9. Tesfaye, M.; Gonfa, Y.; Tadesse, G.; Temesgen, T.; Periyasamy, S. Green synthesis of silver nanoparticles using *Vernonia amygdalina* plant extract and its antimicrobial activities. *Heliyon* **2023**, *9*, e17356. [CrossRef]
10. Elhady, S.S.; Abdelhameed, R.F.; Zekry, S.H.; Ibrahim, A.K.; Habib, E.S.; Darwish, K.M.; Hazem, R.M.; Mohammad, K.A.; Hassanean, H.A.; Ahmed, S.A. VEGFR-mediated cytotoxic activity of *Pulicaria undulata* isolated metabolites: A biological evaluation and in silico study. *Life* **2021**, *11*, 759. [CrossRef]
11. Emam, M.A.; Khattab, H.I.; Hegazy, M.G.A. Assessment of anticancer activity of *Pulicaria undulata* on hepatocellular carcinoma HepG2 cell line. *Tumor Biology* **2019**, *41*, 10. [CrossRef] [PubMed]
12. Mohammed, H.A.; Al-Omar, M.S.; Khan, R.A.; Mohammed, S.A.; Qureshi, K.A.; Abbas, M.M.; Al Rugaie, O.; Abd-Elmoniem, E.; Ahmad, A.M.; Kandil, Y.I. Chemical profile, antioxidant, antimicrobial, and anticancer activities of the water-ethanol extract of *Pulicaria undulata* growing in the oasis of central Saudi Arabian desert. *Plants* **2021**, *10*, 1811. [CrossRef] [PubMed]
13. Foudah, A.I.; Alam, A.; Soliman, G.A.; Salkini, M.A.; Ahmed, E.I.; Yusufoglu, H.S. Pharmacognostical, antioxidant and antimicrobial studies of aerial part of *Pulicaria crispa* (Family: Asteraceae). *Bull. Environ. Pharmacol. Life Sci.* **2015**, *4*, 19–27.
14. Elshiekh, Y.H.; Mona, A. Gas chromatography–mass spectrometry analysis of *Pulicaria crispa* (whole plant) petroleum ether extracts. *Am. J. Res. Commun.* **2015**, *3*, 58–67.
15. Damyeh, M.S.; Niakousari, M. Ohmic hydrodistillation, an accelerated energy-saver green process in the extraction of *Pulicaria undulata* essential oil. *Ind. Crops Prod.* **2017**, *98*, 100–107. [CrossRef]
16. Paramasivam, G.; Palem, V.V.; Sundaram, T.; Sundaram, V.; Kishore, S.C.; Bellucci, S. Nanomaterials: Synthesis and applications in theranostics. *Nanomaterials* **2021**, *11*, 3228. [CrossRef]
17. Baig, N.; Kammakakam, I.; Falath, W. Nanomaterials: A review of synthesis methods, properties, recent progress, and challenges. *Mater. Adv.* **2021**, *2*, 1821–1871. [CrossRef]
18. Karunakaran, G.; Sudha, K.G.; Ali, S.; Cho, E.-B. Biosynthesis of nanoparticles from various biological sources and its biomedical applications. *Molecules* **2023**, *28*, 4527. [CrossRef]
19. Ramakrishna, M.; Rajesh Babu, D.; Gengan, R.M.; Chandra, S.; Nageswara Rao, G. Green synthesis of gold nanoparticles using marine algae and evaluation of their catalytic activity. *J. Nanostruct. Chem.* **2016**, *6*, 1–13. [CrossRef]
20. Rana, A.; Yadav, K.; Jagadevan, S. A comprehensive review on green synthesis of nature-inspired metal nanoparticles: Mechanism, application and toxicity. *J. Clean. Prod.* **2020**, *272*, 122880. [CrossRef]
21. Jadoun, S.; Arif, R.; Jangid, N.K.; Meena, R.K. Green synthesis of nanoparticles using plant extracts: A review. *Environ. Chem. Lett.* **2021**, *19*, 355–374. [CrossRef]
22. Dehvari, M.; Ghahghaei, A. The effect of green synthesis silver nanoparticles (AgNPs) from *Pulicaria undulata* on the amyloid formation in α-lactalbumin and the chaperon action of α-casein. *Int. J. Biol. Macromol.* **2018**, *108*, 1128–1139. [CrossRef] [PubMed]
23. Khan, M.; Al-Hamoud, K.; Liaqat, Z.; Shaik, M.R.; Adil, S.F.; Kuniyil, M.; Alkhathlan, H.Z.; Al-Warthan, A.; Siddiqui, M.R.H.; Mondeshki, M. Synthesis of Au, Ag, and Au–Ag bimetallic nanoparticles using *Pulicaria undulata* extract and their catalytic activity for the reduction of 4-nitrophenol. *Nanomaterials* **2020**, *10*, 1885. [CrossRef] [PubMed]
24. Azwanida, N. A review on the extraction methods use in medicinal plants, principle, strength and limitation. *Med. Aromat. Plants* **2015**, *4*, 2167–2412.
25. Devasenan, S.; Beevi, N.H.; Jayanthi, S. Synthesis and characterization of copper nanoparticles using leaf extract of *Andrographis paniculata* and their antimicrobial activities. *Int. J. ChemTech Res.* **2016**, *9*, 725–730.
26. Otunola, G.A.; Afolayan, A.J.; Ajayi, E.O.; Odeyemi, S.W. Characterization, antibacterial and antioxidant properties of silver nanoparticles synthesized from aqueous extracts of *Allium sativum*, *Zingiber officinale*, and *Capsicum frutescens*. *Pharmacogn. Mag.* **2017**, *13*, S201. [CrossRef]
27. Bhattacharjee, S. DLS and zeta potential–what they are and what they are not? *J. Control. Release* **2016**, *235*, 337–351. [CrossRef]
28. Honary, S.; Zahir, F. Effect of zeta potential on the properties of nano-drug delivery systems-a review. *Trop. J. Pharm. Res.* **2013**, *12*, 265–273.
29. Burlingame, B. Wild nutrition. *J. Food Compos. Anal.* **2000**, *2*, 99–100. [CrossRef]
30. Issa, N.K.; Abdul Jabar, R.; Hammo, Y.; Kamal, I. Antioxidant activity of apple peels bioactive molecules extractives. *J. Sci. Technol.* **2016**, *6*, 76–88.
31. Zhishen, J.; Mengcheng, T.; Jianming, W. The determination of flavonoid contents in mulberry and their scavenging effects on superoxide radicals. *Food Chem.* **1999**, *64*, 555–559. [CrossRef]
32. Kitts, D.D.; Wijewickreme, A.N.; Hu, C. Antioxidant properties of a North American ginseng extract. *Mol. Cell. Biochem.* **2000**, *203*, 1–10. [CrossRef] [PubMed]
33. Parejo, I.; Codina, C.; Petrakis, C.; Kefalas, P. Evaluation of scavenging activity assessed by Co (II)/EDTA-induced luminol chemiluminescence and DPPH·(2, 2-diphenyl-1-picrylhydrazyl) free radical assay. *J. Pharmacol. Toxicol. Methods* **2000**, *44*, 507–512. [CrossRef] [PubMed]

34. Boyanova, L.; Gergova, G.; Nikolov, R.; Derejian, S.; Lazarova, E.; Katsarov, N.; Mitov, I.; Krastev, Z. Activity of Bulgarian propolis against 94 Helicobacter pylori strains in vitro by agar-well diffusion, agar dilution and disc diffusion methods. *J. Med. Microbiol.* **2005**, *54*, 481–483. [CrossRef] [PubMed]
35. Opoku, A.; Geheeb-Keller, M.; Lin, J.; Terblanche, S.; Hutchings, A.; Chuturgoon, A.; Pillay, D. Preliminary screening of some traditional Zulu medicinal plants for antineoplastic activities versus the HepG2 cell line. *Phytother. Res.* **2000**, *14*, 534–537. [CrossRef] [PubMed]
36. Abdallah, H.M.; Mohamed, G.A.; Ibrahim, S.R.; Asfour, H.Z.; Khayat, M.T. Undulaterpene A: A new triterpene fatty acid ester from: *Pulicaria undulata*. *Pharmacogn. Mag.* **2019**, *15*, 671–674. [CrossRef]
37. Al-Hajj, N.Q.M.; Wang, H.; Gasmalla, M.A.; Ma, C.; Thabit, R.; Rahman, M.R.T.; Tang, Y. Chemical composition and antioxidant activity of the essential oil of *Pulicaria inuloides*. *J. Food Nutr. Res.* **2014**, *2*, 221–227. [CrossRef]
38. Mansour, H.F.M. Larvicidal Activity of Essential Oils from *Nigella sativa* L. and *Pulicaria undulata* (L.) CA Mey. against the Mosquito Vectors Anopheles gambiae and Culex quinquefasciatus. Ph.D. Thesis, University of Khartoum, Khartoum, Sudan, 2020.
39. Behera, A.; Awasthi, S. Anticancer, antimicrobial and hemolytic assessment of zinc oxide nanoparticles synthesized from *Lagerstroemia indica*. *BioNanoScience* **2021**, *11*, 1030–1048. [CrossRef]
40. Zeinalipour-Yazdi, C.D.; Willock, D.J.; Thomas, L.; Wilson, K.; Lee, A.F. CO adsorption over Pd nanoparticles: A general framework for IR simulations on nanoparticles. *Surf. Sci.* **2016**, *646*, 210–220. [CrossRef]
41. Sharifi-Rad, M.; Pohl, P.; Epifano, F. Phytofabrication of silver nanoparticles (AgNPs) with pharmaceutical capabilities using *Otostegia persica* (burm.) boiss. leaf extract. *Nanomaterials* **2021**, *11*, 1045. [CrossRef]
42. Assaeed, A.; Elshamy, A.; El Gendy, A.E.-N.; Dar, B.; Al-Rowaily, S.; Abd-ElGawad, A. Sesquiterpenes-rich essential oil from above ground parts of *Pulicaria somalensis* exhibited antioxidant activity and allelopathic effect on weeds. *Agronomy* **2020**, *10*, 399. [CrossRef]
43. Sharifi-Rad, M.; Pohl, P. Synthesis of biogenic silver nanoparticles (Agcl-NPs) using a *Pulicaria vulgaris* gaertn. aerial part extract and their application as antibacterial, antifungal and antioxidant agents. *Nanomaterials* **2020**, *10*, 638. [CrossRef] [PubMed]
44. Tavakoli, R.; Mohadjerani, M.; Hosseinzadeh, R.; Tajbakhsh, M.; Naqinezhad, A. Essential-oil and fatty-acid composition, and antioxidant activity of extracts of *Ficaria kochii*. *Chem. Biodivers.* **2012**, *9*, 2732–2741. [CrossRef]
45. Salama, S.A.; Al-Faifi, Z.E.; El-Amier, Y.A. Chemical composition of *Reichardia tingitana* methanolic extract and its potential antioxidant, antimicrobial, cytotoxic and larvicidal activity. *Plants* **2022**, *11*, 2028. [CrossRef] [PubMed]
46. Zubair Dhabian, S.; Sabeeh Jasim, R. Antioxidant, cytotoxic, and antihemolytic activity of greenly synthesized selenium nanoparticles using *Elettaria cardamomum* Extract. *J. Nanostruct.* **2023**, *13*, 76–85.
47. Dhabian, S.Z.; Jasim, R.S. Anticancer and antioxidant activity of the greenly synthesized zinc nanoparticles composites using aqueous extract of *Withania somnifera* plant. *Egypt. J. Chem.* **2021**, *64*, 5561–5574. [CrossRef]
48. Khorrami, S.; Zarrabi, A.; Khaleghi, M.; Danaei, M.; Mozafari, M. Selective cytotoxicity of green synthesized silver nanoparticles against the MCF-7 tumor cell line and their enhanced antioxidant and antimicrobial properties. *Int. J. Nanomed.* **2018**, *13*, 8013. [CrossRef]
49. Salama, S.A.; Al-Faifi, Z.E.; Masood, M.F.; El-Amier, Y.A. Investigation and biological assessment of *Rumex vesicarius* L. extract: Characterization of the chemical components and antioxidant, antimicrobial, cytotoxic, and anti-dengue vector activity. *Molecules* **2022**, *27*, 3177. [CrossRef]
50. Shirzadi-Ahodashti, M.; Mortazavi-Derazkola, S.; Ebrahimzadeh, M.A. Biosynthesis of noble metal nanoparticles using crataegus monogyna leaf extract (CML@X-NPs, X= Ag, Au): Antibacterial and cytotoxic activities against breast and gastric cancer cell lines. *Surf. Interfaces* **2020**, *21*, 100697. [CrossRef]
51. Hussain, A.; Lakhan, M.N.; Hanan, A.; Soomro, I.A.; Ahmed, M.; Bibi, F.; Zehra, I. Recent progress on green synthesis of selenium nanoparticles—A review. *Mater. Today Sustain.* **2023**, *23*, 100420. [CrossRef]
52. Menon, S.; Shrudhi Devi, K.S.; Agarwal, H.; Shanmugam, V.K. Efficacy of Biogenic Selenium Nanoparticles from an Extract of Ginger towards Evaluation on Anti-Microbial and Anti-Oxidant Activities. *Colloid Interface Sci. Commun.* **2019**, *29*, 1–8. [CrossRef]
53. Sarkar, R.D.; Lahkar, P.; Kalita, M.C. *Glycosmis pentaphylla* (Retz.) DC leaf extract mediated synthesis of selenium nanoparticle and investigation of its antibacterial activity against urinary tract pathogens. *Bioresour. Technol. Rep.* **2022**, *17*, 100894. [CrossRef]
54. Vinu, D.; Govindaraju, K.; Vasantharaja, R.; Amreen Nisa, S.; Kannan, M.; Vijai Anand, K. Biogenic zinc oxide, copper oxide and selenium nanoparticles: Preparation, characterization and their anti-bacterial activity against *Vibrio parahaemolyticus*. *J. Nanostruct. Chem.* **2021**, *11*, 271–286. [CrossRef]
55. El-Zayat, M.M.; Eraqi, M.M.; Alrefai, H.; El-Khateeb, A.Y.; Ibrahim, M.A.; Aljohani, H.M.; Aljohani, M.M.; Elshaer, M.M. The antimicrobial, antioxidant, and anticancer activity of greenly synthesized selenium and zinc composite nanoparticles using *Ephedra aphylla* extract. *Biomolecules* **2021**, *11*, 470. [CrossRef] [PubMed]
56. Chen, Q.; Dharmaraj, T.; Cai, P.C.; Burgener, E.B.; Haddock, N.L.; Spakowitz, A.J.; Bollyky, P.L. Bacteriophage and bacterial susceptibility, resistance, and tolerance to antibiotics. *Pharmaceutics* **2022**, *14*, 1425. [CrossRef]

57. Akter, M.; Sikder, M.T.; Rahman, M.M.; Ullah, A.A.; Hossain, K.F.B.; Banik, S.; Hosokawa, T.; Saito, T.; Kurasaki, M. A systematic review on silver nanoparticles-induced cytotoxicity: Physicochemical properties and perspectives. *J. Adv. Res.* **2018**, *9*, 1–16. [CrossRef] [PubMed]
58. Shaukat, U.; Ahemad, S.; Wang, M.; Khan, S.I.; Ali, Z.; Tousif, M.I.; Abdallah, H.H.; Khan, I.A.; Saleem, M.; Mahomoodally, M.F. Phenolic contents, chemical profiling, in silico and in vitro anti-inflammatory and anticancer properties of *Alnus nitida* (Spach) Endl. *S. Afr. J. Bot.* **2021**, *138*, 148–155. [CrossRef]